Batteries & Supercaps

Research Article
doi.org/10.1002/batt.202200252

Chemistry Europe
European Chemical Societies Publishing

www.batteries-supercaps.org

# A Self-Standing Flexible Gel Polymer Electrolyte for Dendrite-Free Lithium-Metal Batteries

Sweta Mariam George,[a] S. Sampath,*[b] and Aninda J. Bhattacharyya*[c]

We discuss here a self-standing and flexible homogeneous amorphous gel polymer electrolyte (abbreviated as LiGPE) as an alternative electrolyte for lithium-metal batteries. The LiGPE, comprises of a large volume of liquid lithium bis(trifluoromethanesulfonyl) imide (LiTFSI) salt in tetra ethylene glycol dimethyl ether (TEGDME) electrolyte confined inside in situ synthesized network of acrylonitrile and acrylate, which is poly(ethylene glycol) methyl ether methacrylate or PEGME-MA. The glyme-based liquid electrolyte in the LiGPE discussed here, which is completely devoid of ionic liquids, essentially plays the role of a plasticizer. The LiGPE exhibits high room temperature ionic conductivity (2.3 mS cm$^{-1}$), high lithium-transference number of approximately 0.6, good thermal stability (155 °C) and excellent electrochemical properties. At varying current densities, it facilitates a dendrite free plating and de-plating of lithium across its interface for long periods of time. The high oxidative stability against lithium (Li) up to 5.3 V strongly suggests that it will provide a safer operating Li-metal battery compared to conventional liquid electrolytes. The LiGPE, when assembled in Li-metal cell comprising of Li-metal anode and Li-ion insertion cathode material ($LiFePO_4$, LFP), demonstrated excellent stability and delivered 90% of theoretical capacity when cycled over 100 cycles. We discuss here a self-standing and flexible homogeneous amorphous gel polymer electrolyte (abbreviated as LiGPE) as an alternative electrolyte for lithium-metal batteries. The gel shows superior interfacial properties with lithium (Li) metal, supressing dendritic growth and enhancing Li-ion transference number (0.64). The high oxidative stability against Li up to 5.3 V strongly suggests that it will provide a safer operating Li-metal battery. The LiGPE, comprises of a large volume of liquid lithium bis(trifluoromethanesulfonyl) imide (LiTFSI) salt in tetra ethylene glycol dimethyl ether (TEGDME) electrolyte confined inside in-situ synthesized network of acrylonitrile and acrylate, which is poly(ethylene glycol) methyl ether methacrylate or PEGMEMA. The glyme-based liquid electrolyte in the LiGPE discussed here, which is completely devoid of ionic liquids, essentially plays the role of a plasticizer, enhancing the ionic conductivity (2.3 mS cm$^{-1}$) without compromising with the mechanical stability or thermal stability (155 °C) of GPE.

## Introduction

Rechargeable batteries are playing a paramount role in transcending towards a fossil fuel free, greener and sustainable world.[1,2] Lithium-ion rechargeable batteries (LiBs) have revolutionized portable electronics as well as diverse hand-held applications. The electric vehicles have taken off based on LiBs and efforts are on to expand their footprint into mass scale deployment in electric power grids.[3] The immense advances in LiBs have been achieved via discovery of new electroactive materials. However, it has reached its zenith in terms of practical energy and power density, which will be insufficient to meet the energy demands for the near and distant future.[4] One of the important recent strategies to boost energy, without resorting to large scale modifications in the conventional lithium-ion cell, has been to revert from an intercalation based (e.g., graphite) to lithium-metal as the anode. Lithium (Li) metal is attractive owing to its very low molecular weight, very high specific capacity of 3860 mAh g$^{-1}$ and electrochemical potential of −3.04 V (vs. SHE).[5] However, the safety and cyclability of lithium-metal anode batteries operating with liquid electrolytes have always been a formidable challenge.[6,7] While commercial viability of several classes of Li-intercalation cathodes are now well established, availability of thermally and electrochemically stable high ionic conductivity electrolytes continue to be an insurmountable challenge.[8] As electrolyte is the ion transporter between the electrodes which eventually determines the underlying efficiency of the redox process at the electrode, it is befitting to converge focus on the development of alternative electrolytes leading to good substitution for liquid electrolytes.[9]

Irrespective of the battery chemistry, high electrochemical performance and safety can be simultaneously achieved provided the electrolyte is electrochemically compatible in the operation voltage window determined by the cell electrodes.[10] This matter essentially narrows down to the electrolyte properties and its ability to form a stable passivation layer at its interface with the electrode. A solid-liquid interface can

[a] S. M. George
Interdisciplinary Center for Energy Research
Indian Institute of Science
Bangalore, 560012 India
[b] Prof. S. Sampath
Department of Inorganic and Physical Chemistry
Indian Institute of Science
Bangalore, 560 012 India
E-mail: sampath@iisc.ac.in
[c] Prof. A. J. Bhattacharyya
Solid State and Structural Chemistry Unit
Indian Institute of Science
Bangalore, 560012 India
E-mail: anindajb@iisc.ac.in

Supporting information for this article is available on the WWW under https://doi.org/10.1002/batt.202200252

intuitively seem like a good interface for ion exchange.[11] However, lithium being an extremely reactive alkali metal, forms passivation layer of diverse decomposition products of the electrolyte when it meets organic liquid electrolytes.[11,12] Most often, the solid electrolyte interface (SEI) layer formed with liquid electrolyte is not stable and may grow uncontrollably upon consecutive cycling resulting in continuous consumption of lithium and reduction in specific capacity.[13–15] Along with an unstable SEI formed, Li-dendrite formation and growth is a perennial problem leading to severe safety hazards. Organic systems especially polymers provide plentiful opportunities towards the development of high ionic conductivity, electrochemically, thermally and mechanically stable electrolytes. Inorganic solid-state electrolytes overcome these setbacks of liquid electrolytes along with the benefit of suppression of dendrite formation due to high shear modulus.[16–18] However, inorganic solid-state electrolytes are restrained to a few chemical types (e.g., oxides, sulphides),[19] possess low ionic conductivity and high interfacial charge transfer resistance. All these factors are counterproductive for long-life batteries.[20,21] In contrast, organic soft matter electrolytes, especially polymer electrolytes open countless opportunities for the design of electrolytes with optimal properties. Polymer electrolytes can be broadly divided into solid polymer electrolyte (SPE), gel polymer electrolyte (GPE) and composite polymer electrolyte.[22–24] In SPE, due to the lack of solvent molecules, the conduction mechanism remains solely controlled by the segmental motion of the polymer.[25] This restricts its ionic conductivity through the semi crystalline phase and comes with a large electrode|electrolyte interface resistance. In order to improve the ionic conductivity, ceramic and metal oxides nanofillers are incorporated (as 'plasticizers') within the polymer to form composite polymer electrolyte.[26,27] Gel polymer electrolytes, brings together the advantages of high ionic conductivity and good interfacial properties like that of liquid electrolytes. It displays mechanical properties like that of solids with a high degree of flexibility. Depending on the chemical composition and design, a gel polymer system has the potential to outperform the liquid and inorganic solid-state electrolytes leading to a compact, and safe high energy density device.[28,29]

The choice of precursor materials viz. the salt, solvent and monomer/oligomers determine the physical and electrochemical properties of the gel polymer electrolyte. Polymers like polyethylene oxide (PEO), polypropylene oxide (PPO), polyacrylonitrile (PAN), polymethyl methacrylate (PMMA), poly(vinylidene fluoride-hexafluoro propylene) (PVdF-HFP) are some of the well-studied polymer backbones for GPE.[30,31] Polyacrylonitrile (PAN) based polymer electrolytes, both dry solid polymer electrolyte and gel polymer electrolytes has been investigated in literature due to its good electrochemical stability window against lithium, high solvating ability of many lithium salts due to high dielectric constant, good thermal stability, good ionic conductivity. However, the lithium ions bind strongly to the Lewis base polymer nitrile functional group leading to it's strong coordination with the polymer backbone. Thus, the mobility of lithium ions are completely controlled by the changes in the polymer conformation.[32,33] The addition of plasticiser enhances the amorphous nature of the polymer which is mainly known to assist the ionic conduction. The right choice of functional groups in the plasticiser or the copolymer added can decide the strength of coordination of nitrile group to the lithium ions. Carbonyl groups are analogous to nitrile group in terms of the polar pi bonds and possesses a stronger electronegative –O group compared to the nitrile-N. Hence, when nitrile and carbonyl pendant groups are both present, they compete to coordinate with the lithium ions. The repulsive interaction between the functional groups eventually leads to an environment where the lithium ions are significantly freer and available for fast conduction.[34]

We report here a gel polymer electrolyte comprising of a physical network of PAN and poly(ethylene glycol)methyl ether methacrylate (PEGMEMA) polymers confining tetraglyme(TEGDME)-Li-salt as the plasticiser. The tetraglyme, by virtue of its high donor number and strong Lewis basicity (due to lone pair of electrons on oxygen) enhances ion-dissociation.[35] A careful optimisation of ratios of acrylate (PEGMEMA), acrylonitrile (PAN) and the lithium liquid electrolyte containing LiTFSI in TEGDME in the GPE ensured that a high ionic conductivity is achieved along with formation of a free standing, transparent gel. The carbonyl functionality of the acrylate polymer, oxygen from the glyme plasticiser and nitrile functionality in PAN compete for coordination with lithium, decoupling it from all and making higher number of lithium available for conduction. This can be seen from the high transference number of lithium obtained in the GPE reported in this work. A large volume of LiTFSI in TEGDME plasticiser securely confined in the network of polymers, forms an extremely compatible interface with lithium as evident from the EIS, symmetric cell cycling studies as well as galvanostatic cycling with well-known Li- insertion electrodes.

## Results and Discussion

**Ionic conductivity and transference number of lithium**: The synthesized gel polymer electrolyte comprises of a network of polyacrylonitrile (PAN) and PEGMEMA which confines the liquid electrolyte comprising of LiTFSI salt in TEGDME (Scheme 1). Along with high ionic conductivity, a mechanically stable, free-standing gel is preferred for the ease of cell assembly and safety. To obtain the best composition of gel polymer electrolyte with good ionic conductivity and mechanical stability, different volume ratios of acrylonitrile and PEGMEMA are in-situ polymerised in the presence of the lithium liquid electrolyte (1 M LiTFSI in TEGDME). The conductivity of the gels is calculated using electrochemical impedance spectroscopy in a stainless-steel blocking electrode setup (Figure S1 and Table S1). The bulk resistance of the electrolyte obtained from the high frequency data point is used to calculate the ionic conductivity of the gels (Supporting Information Equation S(1)).[36] The composition of AN: PEGMEMA = 2 : 1 (v/v) formed a

Research Article
doi.org/10.1002/batt.202200252
Chemistry Europe
European Chemical Societies Publishing

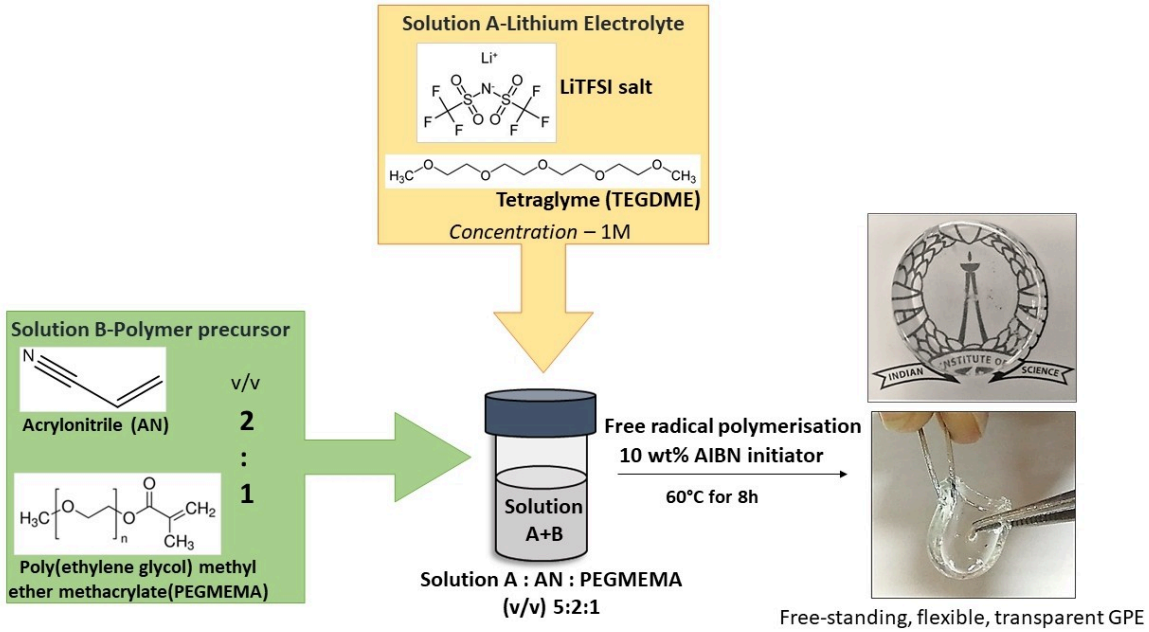


**Scheme 1.** Schematic representation of the synthesis of Li-GPE.

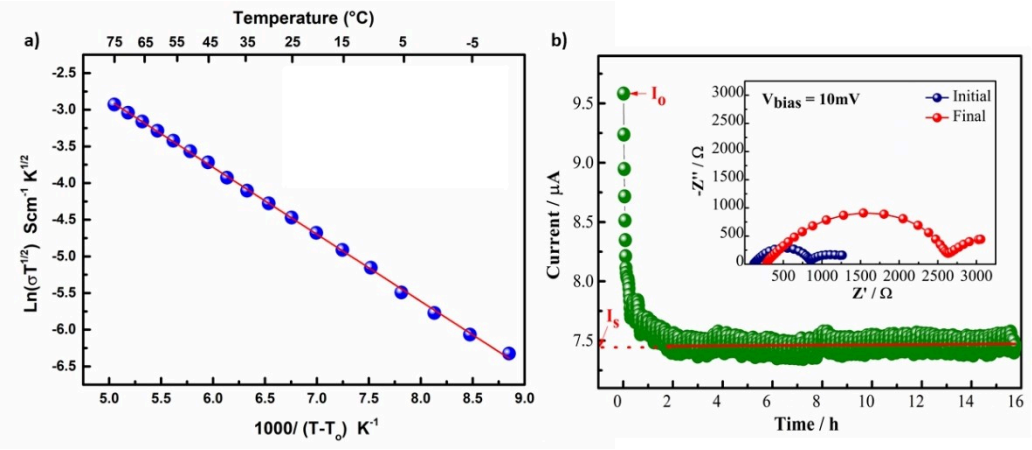


**Figure 1.** a) The VTF fit of temperature dependent ionic conductivity of Li-GPE. b) Chronoamperometry showing the variation of current versus time of a lithium symmetric cell having Li-GPE sandwiched between lithium non-blocking electrodes. Inset: Nyquist plot from AC-impedance spectroscopy measured before and after the chronoamperometric measurements (bias = 10 mV for 16 h).

flexible, free standing, transparent gel with a very promising ionic conductivity of 2.3 mS cm$^{-1}$.

Further, the ionic conductivity is studied as a function of temperature over the temperature range (−5 to 75) °C (Figure 1a). The curvature observed in the temperature dependent ionic conductivity (Figure S2) is generally a characteristic of amorphous systems. This arises due to free volume changes, which is conventionally analysed using the Vogel-Tamman-Fucher (VTF) model (Equation S(2)).[37,38] The amorphous nature of the gel can be also inferred from the broad hump-like feature observed at $2\theta = 20°$ in the X-ray diffractogram shown in (Figure S3).[38] The morphology of the gel, observed using scanning electron microscope, shows a dense amorphous solid without any phase separation (Figure S4). The presence of glyme results in a plasticising effect giving rise to a completely amorphous gel at room temperature. This enables a fast-ion conduction pathway.[39,40] The slope of the straight line fit (Figure 1a) using the VTF equation gives the (pseudo)activation energy. The (pseudo)activation energy signifies ion mobility which occurs because of free volume rearrangement resulting due to polymer segmental motion.[3] The activation energy for ion conduction through this system is calculated to be 0.08 eV (= 7.7 kJ mol$^{-1}$). This low barrier for activation and free lithium ions for conduction will expectedly make transport of lithium-ion easier and hence improve the lithium ion transference number.[41]

Low lithium transference number below 0.5 has been matter of great concern in polymer electrolyte research.[42]

Research Article
doi.org/10.1002/batt.202200252
Chemistry Europe
European Chemical Societies Publishing

Figure 1(b) depicts the lithium-ion transference number measured using the modified Bruce, Evans and Vincent method[43] (Equation S3, Supporting Information) which uses a symmetric cell comprising of Li-GPE sandwiched between lithium non-blocking electrodes. The initial current obtained upon application of a small bias of 10 mV is due to both anions and cations. The current drops exponentially to a saturation value, which is only due to lithium-ions. The charge transfer resistance across the interface before and after the chronoamperometry, measured using ac-impedance spectroscopy, resulted in a lithium transference number of approximately 0.64. A high transference number of lithium is advantageous as it contributes towards the formation of a stabile SEI against the lithium metal anode and avoids the formation of concentration gradient within the electrolyte. These factors lead to an overall improvement in cyclability and health of the battery.[15,44]

**Mechanical stability**: While the ionic conductivity and lithium-ion transference number improves following the incorporation of a large volume of plasticiser in the LiGPE, the mechanical stability of the system should not be compromised. Extensive studies are performed to ascertain the mechanical stability of the gel polymer electrolytes. This is observed in the stress-strain curve of Li-GPE from the compression test on Li-GPE in Figure 2. The synthesised GPE shows a remarkable compression modulus of 0.54 MPa and an ultimate compression strength of 1.2 MPa at 73.5% strain. The gel retains its shape while under compression and slowly regains initial dimensions if load is removed at low strains (Figure 2 inset). Mechanical stability under compression and good rheological properties are essential for a good assembly and cyclability of a polymer battery. A mechanical failure can lead to increase in charge transfer resistance, and hence degrade the battery performance.[45]

The strain amplitude sweep of the LiGPE is performed over a range of 0.01% to 100% shear strain at the fixed angular frequency of 10 rad/s (Figure 3a). The storage modulus ($G'$) and loss modulus ($G''$) is measured to be a constant value independent of shear strain up to the critical strain ($\gamma_c$) of

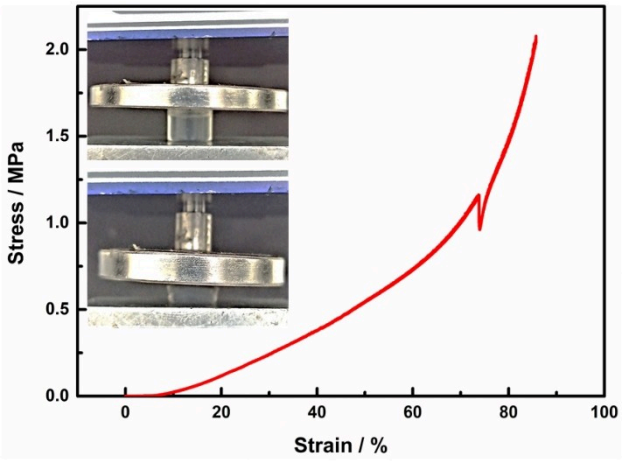


**Figure 2.** The compression stress-strain curve of LiGPE; inset: photographs of LiGPE before compression (top) and during compression test (bottom)

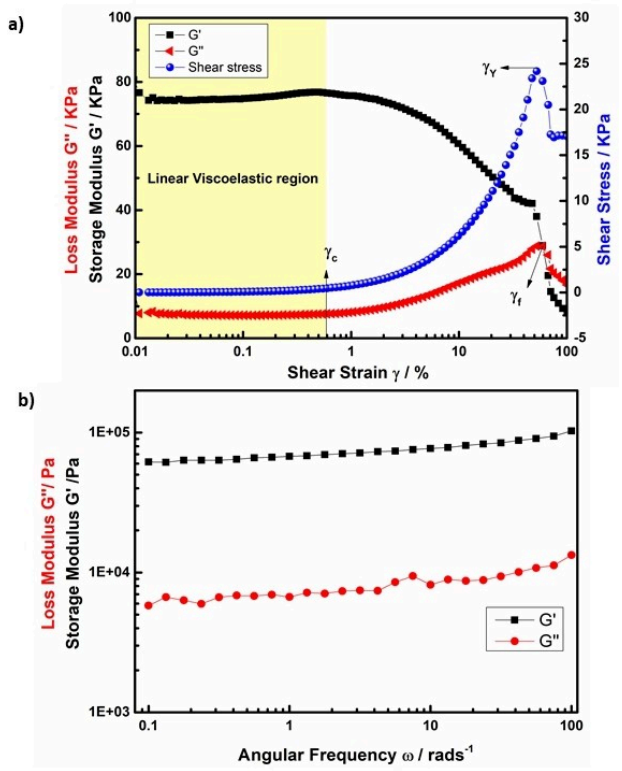


**Figure 3.** a) Strain-amplitude sweep of the lithium gel polymer electrolyte at angular frequency of 10 rad/s; b) frequency sweep test performed on lithium gel polymer electrolyte at fixed shear strain of 0.1%.

0.58%. This region from 0.01% to the critical stain value is called the linear viscoelastic region (LVER). In LVER, the value of $G'$ is more than 10 times higher than $G''$ confirming the gel like-viscoelastic solid nature of the electrolyte reported. The $G'$ value in the LVER gives the stiffness of material or gel strength of 77 kPa in shear condition. The shear stress is also observed to be a constant value in the LVE region. On increasing the shear strain beyond the critical shear stress value, the $G'$ value gradually decreases implying a gradual breakdown of the gel material. The gradual increase in $G''$ value shows that micro-cracks appear in the material first, followed by a propagation of cracks throughout the material when the loss modulus attains a maximum. At the maximum value of $G''$, storage modulus becomes equal to loss modulus and the viscoelasticity of the material is taken over by fluid like behaviour. The shear strain of fluidization is measured as $\gamma_f = 59.6\%$. The nature of loss modulus curve attaining a distinct maximum during the amplitude strain sweep shows that the gel formed a consistent, three-dimensional network. The shear stress corresponding to fluidization point is 23 kPa. The curve of shear stress versus shear strain attains a maximum after the LVER called the yield point, denoted by $\gamma_Y$ in the graph. The yielding shear and strain values are 24.2 kPa and 53.6% respectively. The storage modulus $G'$ is an order greater than loss modulus $G''$ throughout the angular frequency region of 0.1–100 rad/s showing a viscoelastic behaviour over the entire range (Figure 3b). The curves of $G'$ and $G''$ are parallel and shows

Research Article
doi.org/10.1002/batt.202200252
Chemistry Europe
European Chemical Societies Publishing

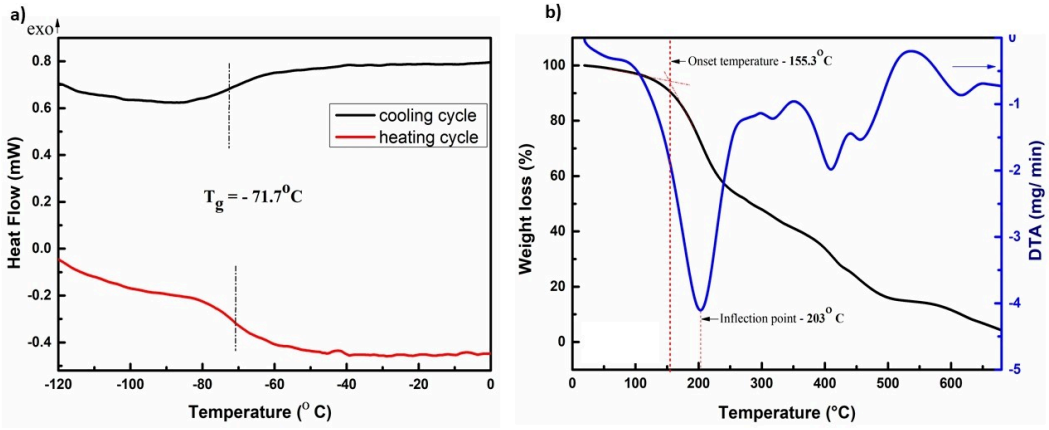


**Figure 4.** a) Differential scanning calorimetry (DSC) curve of completely amorphous gel showing the glass transition temperature of the Li-GPE in the cooling and heating cycles. b) Thermogravimetric analysis (TGA) and differential thermal analysis (DTA) curves depicting the onset and inflection temperature of the weight loss of Li-GPE.

negligible increase over the entire frequency sweep range which are properties of a strong gel.[46]

**Thermal and electrochemical stability**: The plasticising effect of the tetraglyme gives rise to a completely amorphous gel at room temperature enabling fast ion conduction pathways, which are decoupled from the polymer backbone.[47] Differential scanning calorimetry measurements reveal a very low glass transition temperature at −72 °C, above which the polymer transforms to the viscoelastic phase state facilitating fast ion transport (Figure 4a). Almost 60 % of the volume of the free-standing gel comprises of the lithium salt liquid electrolyte and this is well confined inside the physical gelled network of acrylate and acrylonitrile polymers (FTIR spectrum in Figure S5). The liquid solvent will expectedly minimize the coordination of the Li-ions to the nitrile pendant groups of the polyacrylonitrile giving rise to a predominantly liquid solvent mediated conduction of the Li-ions. In addition, the competitive binding carbonyl groups on the acrylate polymer will further reduce the tendency of the nitrile to coordinate $Li^+$.[34] Despite confining a high volume of liquid lithium electrolyte, the thermal stability of the electrolyte is however, not compromised. The thermogravimetric analysis of the Li-GPE shows no weight loss up to 155.3 °C and has an inflection point of 203 °C (Figure 4b).

Apart from the thermal stability of an electrolyte, an oxidative stability voltage higher than the operative voltage range of the cathode immensely contributes to the safety aspects of the battery.[48] Figure 5 shows the linear sweep voltammogram to ascertain the anodic breakdown limit of the Li-GPE assembled with lithium and stainless-steel electrodes. The proposed gel polymer electrolyte showed a good oxidative stability up to 5.3 V. This is higher than most of the operation voltage range of Li-intercalation cathodes reported[49,50] and hence can be compatible with high voltage lithium-ion battery cathodes. In contrast, the oxidative stability of the liquid electrolyte 1 M LiTFSI in TEGDME is low, equal to 3.7 V (Figure 5 inset). The confinement of this liquid electrolyte inside the proposed gel greatly improves the electrochemical stability window of the electrolyte.

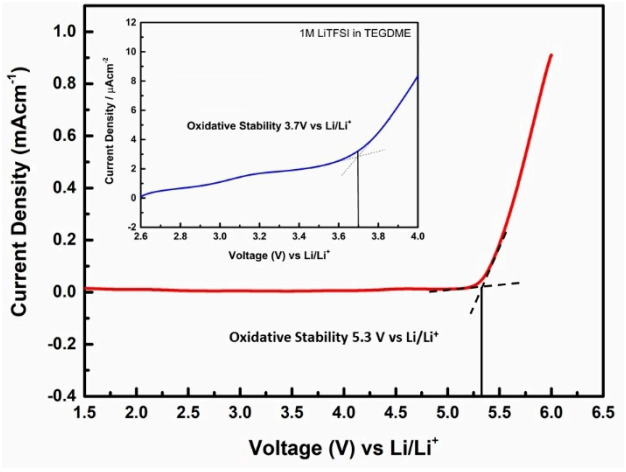


**Figure 5.** Linear sweep voltammogram depicting the anodic breakdown voltage limit of LiGPE and liquid electrolyte 1 M LiTFSI in TEGDME (inset)

Along with the oxidative stability of the GPE, the stability of lithium stripping and plating across the electrolyte interface also plays an important role in the cyclability of the battery. The use of lithium metal in batteries is advantageous due to the high specific capacity offered by the lithium metal owing to its low molecular weight. However, the high possibility of formation of lithium dendrites on repeated stripping and plating is a persistent problem. Uncontrolled growth of dendrites is a serious safety hazard and can lead to shorting of the anode and cathode.[51,52] The profile and overpotential values from a galvanostatic charge and discharge experiment performed in a symmetric lithium cell can help in excluding the effects from any other non-lithium metal interfaces with electrolyte. A lithium symmetric cell with electrolyte, thus, solely give information about the interfacial stability of lithium with the synthesised electrolyte during stripping and plating. Figure 6 shows the galvanostatic stripping and plating of a symmetric lithium cell assembled with the gel polymer electrolyte. The charge and discharge which corresponds to stripping

Research Article
doi.org/10.1002/batt.202200252
Chemistry Europe
European Chemical Societies Publishing

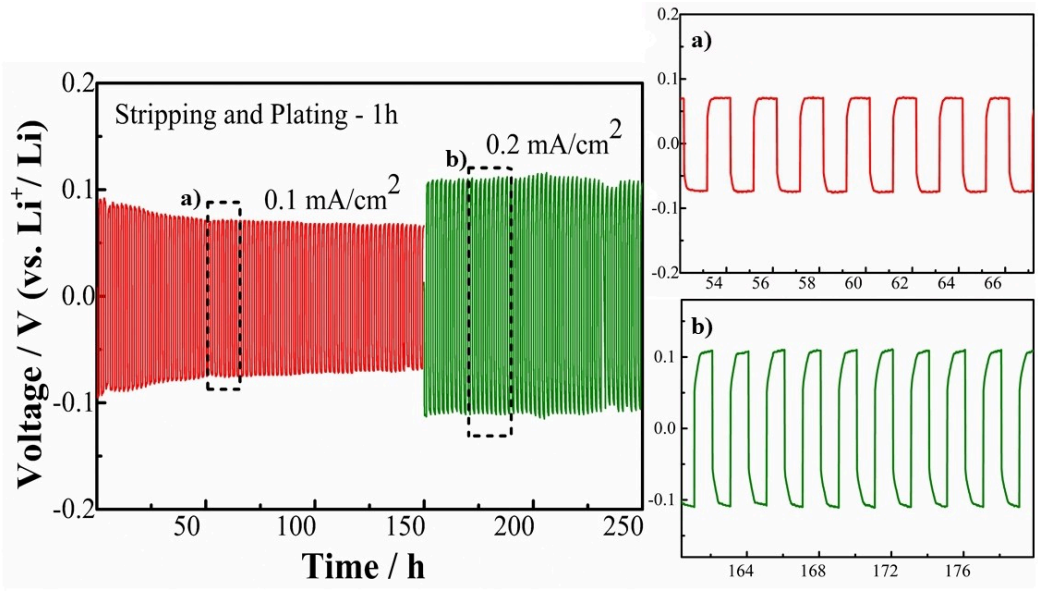


**Figure 6.** Galvanostatic stripping and plating of lithium in a lithium symmetric cell at different current rates for 250 h. a and b) shows the enlarged profile of the symmetric cell cycling at current densities 0.1 mA cm$^{-2}$ and 0.2 mA cm$^{-2}$, respectively.

and plating is done for 1 h each at current densities of 0.1 mA cm$^{-2}$ and 0.2 mA cm$^{-2}$ at 25 °C. Stable overpotential profiles of 69 mV is observed for about 150 h when cycled at 0.1 mA cm$^{-2}$ and the overpotential at 0.2 mA cm$^{-2}$ is 110 mV. The low overpotentials indicates lower hindrance to the kinetics of stripping and plating across the interface of lithium formed with the Li-GPE.[53] The zoomed in portions of galvanostatic stripping and plating profile in Figure 6(a and b) reveal a flat plateau at a small overpotential value can be observed at both the current densities. The absence of peaking behaviour in the voltage-time profiles indicates absence of pitting and dendrite growth.[54] The SEM images of lithium before and post cycling in Figures S6 and S7 respectively confirms that the Li-GPE facilitates a dendrite-free plating of lithium. In contrast, SEM image of lithium from a symmetric cell cycled with the liquid electrolyte 1 M LiTFSI-TEGDME, at the same current density over the same period of time as that of (Li|Li-GPE|Li) cell shows needle-like dendritic growth throughout the surface along with pits formed during non-uniform pitting (Figure S8).

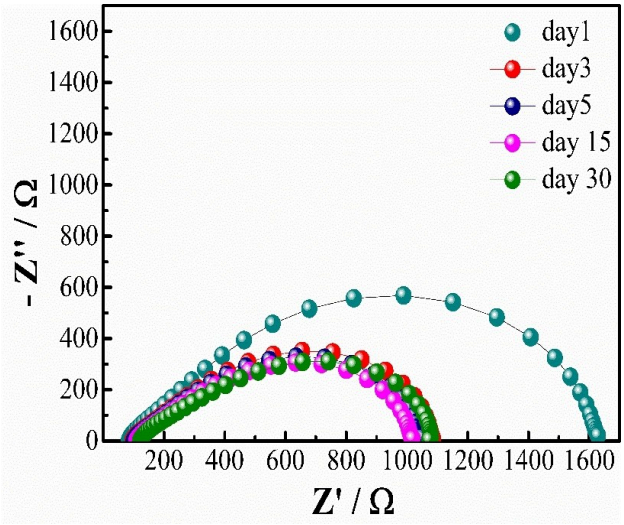


**Figure 7.** Nyquist plots from ac impedance measurement of symmetric lithium cell assembled with synthesised polymer electrolyte studied over a period of 30 days.

**Stability of interface with lithium**: A passivation layer is formed almost instantly when an electrolyte is kept in contact with lithium metal. This layer formed, known as the solid electrolyte interface (SEI), allows Li-ion transport across it while restricting electron transport and hence protects the electrolyte from further decomposition.[55] The stability and ionic conductivity of the solid electrolyte interface (SEI) formed between the lithium and electrolyte greatly contributes to the overpotential in the electro dissolution and deposition of lithium.[56]

Electrochemical impedance spectroscopy (EIS) is used to probe the stability of SEI formed between lithium metal and synthesised GPE for over a 1-month period. Figure 7 shows the Nyquist plots obtained from the ac-impedance measurements on a lithium symmetric cell with the GPE sandwiched in-between. The electrical circuit used to fit the impedance data along with the fitting parameters are shown in the Figure S9 and Table S2, Supporting Information. It is interesting to note that in the low frequency region, which provides information regarding the charge transfer resistance offered by the passivation layer for ion transport, the resistance decreases after day 1 to 1060 Ω and does not change significantly even after 30 days. This implies that the interface of the Li|Li-GPE is highly stable. Further, the bulk resistance of the electrolyte is observed to be stable throughout the period of measurement. The high frequency region of the impedance spectrum, which is a straight line with slope ≈45° and relates to diffusion across a finite length, can be modelled using a finite length Warburg

diffusion element. The EIS study indicates that symmetrical cell assembled with lithium and GPE forms a homogenous passivation layer formed at the interface enabling a planar diffusion of cations.[57,58]

The commendable compatibility of the synthesised gel polymer electrolyte with lithium metal anode in terms of interfacial stability, efficient Li-metal dissolution and deposition, good oxidative stability (≈5 V) calls for further probing of the electrochemical performance in a Li-metal cell with a commercial cathode material. Figure 8 shows the cyclic voltammogram, galvanostatic charge and discharge cycling of the Li-GPE with Li-metal anode and lithium iron phosphate (LFP) cathode. The battery assembled does not contain any additional separator or liquid electrolyte. The cyclic voltammograms in Figure 8(a) show high reversibility of the $Fe^{2+}||Fe^{3+}$ redox couple ($Fe^{2+}\rightarrow Fe^{3+}$: 3.7 V vs. $Li/Li^+$; $Fe^{3+}\rightarrow Fe^{2+}$: 3 V vs. $Li/Li^+$).[59,60] The voltage difference between the oxidation peak and reduction peak decreases after each subsequent cycles indicating a reduction in the polarisation due to formation of an efficient interface with the gel polymer electrolyte. The compatibility of the GPE with the LFP cathode is evident from the high-capacity retention (Figure 8b). The Li-metal-LFP battery assembled with the synthesised Li-GPE shows almost 90% of the theoretical capacity up to 100 cycles, cycled at 25 °C. The columbic efficiency of the cell is also observed to be close to 100% throughout the cycling at C/20 current rate. The cycling at higher current rates is shown in Figure S10. The cell shows good rate capability performance regaining the initial capacity when the current is reversed to C/20. The LFP cell with Li-GPE showed stable cycling at higher temperatures of 50 °C and 80 °C as well (Figure S11). Apart from LFP insertion cathode, lithium nickel cobalt aluminium oxide NCA ($LiNi_{0.8}Co_{0.15}Al_{0.05}O_2$) material is also highly sort after because of its high gravimetric energy density.[61] In order to check the versatility of the GPE synthesised, it was assembled against high voltage NCA cathode with lithium metal as anode. Figure S12 shows the initial few cycles of battery cycling. The high first discharge capacity of 200 mAh g$^{-1}$ and the first charge capacity is 190 mAh g$^{-1}$ displays the compatibility and good ion conduction pathway provided by Li-GPE along with the stability of the electrolyte at high voltage battery application. However, there is a capacity loss observed due to the high de-lithiation from the NCA cathode which is reported to have parasitic effects of oxygen loss from the surface and disordering of layered structure from $R\bar{3}m$ to $Fd\bar{3}m$ (disordered spinel) to $Fm\bar{3}m$ (disordered rock salt). These phase transformations lead to inhomogeneous lithium-ion transport in the subsequent cycles leading to low columbic efficiency.[62,63] Structural optimisation of the cathode to improve the columbic efficiency is beyond the scope of this paper. Here, we intend to solely discuss the properties of gel polymer electrolyte and demonstrate its application in a Li-cell.

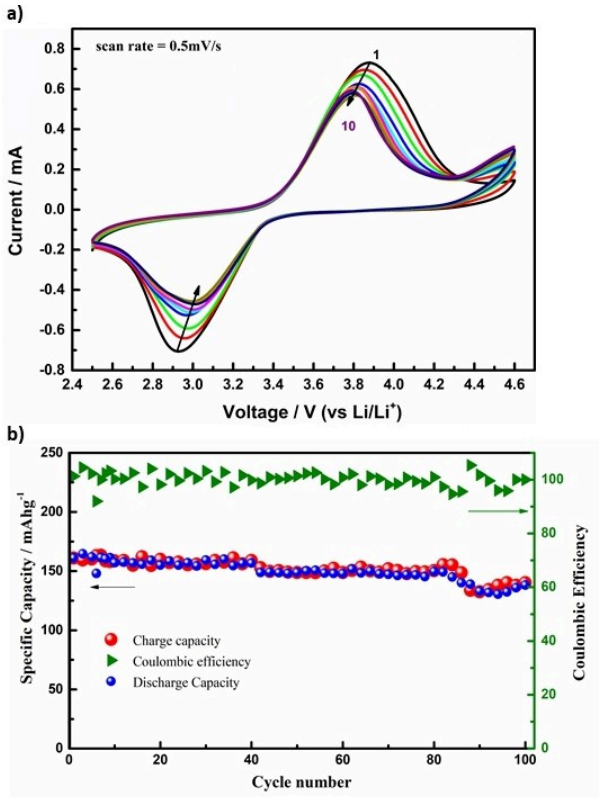


**Figure 8.** a) The cyclic voltammogram of the Li|Li-GPE|LFP cell showing the peaks of the $Fe^{2+}||Fe^{3+}$. b) The specific capacity and coulombic efficiency of the Li|Li-GPE|LFP cell obtained from galvanostatic cycling.

## Conclusion

To conclude, the gel polymer electrolyte discussed here displays excellent mechanical strength, rheological properties and high electrochemical stability towards lithium even with a high fraction (≈60% volume percentage) of the liquid electrolyte confined inside the polymer matrix. Proper choice of materials selection resulted in a fully homogenous amorphous polymer electrolyte with high ionic conductivity and high Li-transference number. The Li-GPE demonstrated excellent redox reversibility and dendrite free stripping and plating of lithium. The robustness of the interfaces formed by the GPE is further exemplified by high specific capacity retention and coulombic efficiency when assembled in a cell with Li-metal anode and well-known insertion cathodes. The Li-GPE discussed here yet again demonstrates the versatility of organic matter in the design of excellent novel ionic conductors. In addition, organic matter provides a paradigm for exploration and design of new cell configurations for various applications, which can otherwise be quite challenging for inorganic solid state ion conductors.

## Materials and Methods

***Chemical details***: Lithium bis(trifluoromethanesulfonyl) imide (LiTFSI) salt, tetra ethylene glycol dimethyl ether (TEGDME), acrylonitrile, poly(ethylene glycol) methyl ether methacrylate (PEGMEMA) of average $M_n$ 500 and 2,2′-azobis(2-methylpropionitrile) (AIBN) of highest purity are purchased from Sigma Aldrich and used as received. Carbon coated lithium iron phosphate of commercial grade is purchased from BAT-SOL equipments and technology.

***Synthesis of gel electrolyte***: 1 M solution of lithium bis(trifluoromethanesulfonyl) imide (LITFSI) salt in tetra ethylene glycol dimethyl ether (TEGDME) is prepared in an argon filled glove box ($H_2O < 1$ ppm; $O_2 < 1$ ppm). Different volume ratios of acrylonitrile (AN) monomer and low molecular weight poly (ethylene glycol) methyl ether methacrylate (PEGMEMA) is added to the solution and stirred to form a homogeneous mixture. 2,2′-azobis(2-methylpropionitrile) (AIBN) (10 wt%) is used as the free radical initiator to polymerise the mixture by solution casting at 60 °C inside the glove box. A flexible, free standing transparent gel polymer electrolyte is obtained after 8 h of polymerisation. Out of the different compositions prepared, the volume ratio of 5 : 2 : 1 of 1 M-LiTFSI/TEGDME: AN: PEGMEMA respectively gives the mechanically stable GPE with the best ionic conductivity value. A schematic explanation of the synthesis procedure is given in Scheme 1.

***Structural characterization:*** The surface morphology and thickness of the synthesised lithium gel polymer electrolyte (LiGPE) are examined using scanning electron microscopy (SEM; (Ultra55 FESEM Karl Zeiss). The powder X-ray diffractogram (PXRD) data of the gel is collected in Panalytical diffractometer using Cu-$K_\alpha$ radiation ($\lambda = 1.54$ Å). The Fourier transform infrared (FTIR) spectroscopy measurements of the gels are recorded using a Bruker Invenio-R diffractometer at a spectral resolution of 4 $cm^{-1}$ in attenuated total reflection (ATR) mode. The mechanical stability of the LiGPE under compression is tested in a Mecmesin micro-universal testing (UTM) machine by with 500N load head displaced at the rate 1 mm/min. The Rheological properties of gel synthesised is tested in Anton Paar modular compact rheometer MCR 302 in the parallel plate geometry The rheological measurements are carried out at room temperature.

***Thermal characterization:*** The glass transition temperature of the LiGPE is determined by differential scanning calorimetry (DSC) in Mettler Toledo DSC 823$^e$ instrument. The decomposition temperature and thermal stability is studied using thermogravimetric analysis (TGA) with TGA/SDTA851$^e$, Mettler Toledo.

***Electrochemical characterization:*** The synthesised gel polymer electrolyte is cut into disc of diameter equal to 11 mm and sandwiched between stainless steel discs of the same diameter in a Swagelok™ cell about ionic conductivity measurement of the Li-GPE. The stainless-steel discs act as blocking electrodes in this configuration. The ionic conductivity is measured by impedance spectroscopy using a Novacontrol Alpha-A impedance analyser in the frequency range 1 Hz to 1 MHz using an output voltage 10 mV. The same instrument is used to ascertain the interfacial stability of the Li-GPE with lithium over a period of 30 days in a lithium symmetric cell. The electrochemical stability window of the GPE was estimated using cyclic voltammetry in a two-electrode configuration assembled in a Swagelok™ cell with Li metal as the pseudo-reference and counter electrode, stainless steel as the working electrode with Li-GPE sandwiched in between the two electrodes. The cyclic voltammetry experiment is performed in CHI 645D electrochemical workstation at room temperature at a scan rate of 5 $mV\,s^{-1}$ over a voltage range −1 V to 5.5 V. The transference number is estimated using a lithium symmetric cell configuration with GPE sandwiched between lithium discs on either side in a Swagelok cell. The technique requires a combination of chronoamperometry with a small voltage bias of 10 mV and impedance spectroscopy sequentially carried out using CHI 645D electrochemical workstation. The efficiency of the stripping and plating of lithium at the interface with GPE is tested in a symmetric lithium cell configuration assembled in a Swagelok™ and cycled in Arbin electrochemical workstation.

## Acknowledgements

*SMG acknowledges Indian Institute of Science (Ministry of Education (MoE), Government of India) for Senior Research Fellowship (SRF) and DST/INT/DFG/P-04/2021 for financial support. AJB acknowledges the financial support from DST, Government of India under the DST/TMD/MECSP/2K17/07. AJB and SS acknowledges SERB-IRHPA (IPA/2021/000007) for project funding.*

## Conflict of Interest

The authors declare no conflict of interest.

## Data Availability Statement

Research data are not shared.

**Keywords:** gel polymer electrolyte · lithium metal battery · interfacial stability · suppressed dendritic growth

[1] J. B. Goodenough, *Energy Storage Mater.* **2015**, *1*, 158–161.
[2] F. Arshad, L. Li, K. Amin, E. Fan, N. Manurkar, A. Ahmad, J. Yang, F. Wu, R. Chen, *ACS Sustainable Chem. Eng.* **2020**, *8*, 13527–13554.
[3] E. C. Evarts, *Nature* **2015**, *526*, S93-S95.
[4] N.-S. Choi, Z. Chen, S. A. Freunberger, X. Ji, Y.-K. Sun, K. Amine, G. Yushin, L. F. Nazar, J. Cho, P. G. Bruce, *Angew. Chem. Int. Ed.* **2012**, *51*, 9994–10024; *Angew. Chem.* **2012**, *124*, 10134–10166.
[5] J. Liu, Z. Bao, Y. Cui, E. J. Dufek, J. B. Goodenough, P. Khalifah, Q. Li, B. Y. Liaw, P. Liu, A. Manthiram, Y. S. Meng, V. R. Subramanian, M. F. Toney, V. V. Viswanathan, M. S. Whittingham, J. Xiao, W. Xu, J. Yang, X.-Q. Yang, J.-G. Zhang, *Nat. Energy* **2019**, *4*, 180–186.
[6] W. Wang, F. Hao, P. P. Mukherjee, *ACS Appl. Mater. Interfaces* **2020**, *12*, 556–566.
[7] Z. Hu, G. Li, A. Wang, J. Luo, X. Liu, *Batteries & Supercaps* **2020**, *3*, 331–335.
[8] B. Horstmann, J. Shi, R. Amine, M. Werres, X. He, H. Jia, F. Hausen, I. Cekic-Laskovic, S. Wiemers-Meyer, J. Lopez, D. Galvez-Aranda, F. Baakes, D. Bresser, C.-C. Su, Y. Xu, W. Xu, P. Jakes, R.-A. Eichel, E. Figgemeier, U. Krewer, J. M. Seminario, P. B. Balbuena, C. Wang, S. Passerini, Y. Shao-Horn, M. Winter, K. Amine, R. Kostecki, A. Latz, *Energy Environ. Sci.* **2021**, *14*, 5289–5314.
[9] R. Usiskin, J. Maier, *Adv. Energy Mater.* **2021**, *11*, 2001455.
[10] Q. Ma, J. Yue, M. Fan, S.-J. Tan, J. Zhang, W.-P. Wang, Y. Liu, Y.-F. Tian, Q. Xu, Y.-X. Yin, Y. You, A. Luo, S. Xin, X.-W. Wu, Y.-G. Guo, *Angew. Chem. Int. Ed.* **2021**, *60*, 16554–16560.
[11] E. Markevich, G. Salitra, D. Aurbach, *ACS Energy Lett.* **2017**, *2*, 1337–1345.
[12] F. Ospina-Acevedo, N. Guo, P. B. Balbuena, *J. Mater. Chem. A* **2020**, *8*, 17036–17055.
[13] X. He, D. Bresser, S. Passerini, F. Baakes, U. Krewer, J. Lopez, C. T. Mallia, Y. Shao-Horn, I. Cekic-Laskovic, S. Wiemers-Meyer, F. A. Soto, V. Ponce, J. M. Seminario, P. B. Balbuena, H. Jia, W. Xu, Y. Xu, C. Wang, B. Horstmann, R. Amine, C.-C. Su, J. Shi, K. Amine, M. Winter, A. Latz, R. Kostecki, *Nat. Rev. Mater.* **2021**, *6*, 1036–1052.
[14] K. Leung, F. Soto, K. Hankins, P. B. Balbuena, K. L. Harrison, *J. Phys. Chem. C* **2016**, *120*, 6302–6313.
[15] L.-T. Wu, S. Nachimuthu, D. Brandell, J.-C. Jiang, *Batteries Supercaps* **2022**, *n/a*.
[16] X. Tian, Y. Yi, B. Fang, P. Yang, T. Wang, P. Liu, L. Qu, M. Li, S. Zhang, *Chem. Mater.* **2020**, *32*, 9821–9848.
[17] H. Liu, X.-B. Cheng, J.-Q. Huang, H. Yuan, Y. Lu, C. Yan, G.-L. Zhu, R. Xu, C.-Z. Zhao, L.-P. Hou, C. He, S. Kaskel, Q. Zhang, *ACS Energy Lett.* **2020**, *5*, 833–843.

[18] M. Golozar, A. Paolella, H. Demers, S. Savoie, G. Girard, N. Delaporte, R. Gauvin, A. Guerfi, H. Lorrmann, K. Zaghib, *Sci. Rep.* **2020**, *10*, 18410.
[19] J. Wolfenstine, J. L. Allen, J. Sakamoto, D. J. Siegel, H. Choe, *Ionics* **2018**, *24*, 1271–1276.
[20] J. A. Dawson, P. Canepa, M. J. Clarke, T. Famprikis, D. Ghosh, M. S. Islam, *Chem. Mater.* **2019**, *31*, 5296–5304.
[21] K. J. Kim, M. Balaish, M. Wadaguchi, L. Kong, J. L. M. Rupp, *Adv. Energy Mater.* **2021**, *11*, 2002689.
[22] L. Long, S. Wang, M. Xiao, Y. Meng, *J. Mater. Chem. A* **2016**, *4*, 10038–10069.
[23] K. S. Ngai, S. Ramesh, K. Ramesh, J. C. Juan, *Ionics* **2016**, *22*, 1259–1279.
[24] S. Qian, H. Chen, Z. Wu, D. Li, X. Liu, Y. Tang, S. Zhang, *Batteries & Supercaps* **2021**, *4*, 39–59.
[25] X. C. Chen, R. L. Sacci, N. C. Osti, M. Tyagi, Y. Wang, J. K. Keum, N. J. Dudney, *Front. Chem.* **2021**, *8*.
[26] S. Rajendran, O. Mahendran, R. Kannan, *J. Phys. Chem. Solids* **2002**, *63*, 303–307.
[27] S. Tang, W. Guo, Y. Fu, *Adv. Energy Mater.* **2021**, *11*, 2000802.
[28] S. Park, B. Jeong, D.-A. Lim, C. H. Lee, K. H. Ahn, J. H. Lee, D.-W. Kim, *ACS Appl. Mater. Interfaces* **2020**, *12*, 19553–19562.
[29] X. Yu, A. Manthiram, *Energy Environ. Sci.* **2018**, *11*, 527–543.
[30] V. Bocharova, A. P. Sokolov, *Macromolecules* **2020**, *53*, 4141–4157.
[31] V. Di Noto, S. Lavina, G. A. Giffin, E. Negro, B. Scrosati, *Electrochim. Acta* **2011**, *57*, 4–13.
[32] P. Hu, J. Chai, Y. Duan, Z. Liu, G. Cui, L. Chen, *J. Mater. Chem. A* **2016**, *4*, 10070–10083.
[33] B. Huang, Z. Wang, L. Chen, R. Xue, F. Wang, *Solid State Ionics* **1996**, *91*, 279–284.
[34] Z. Wang, B. Huang, R. Xue, X. Huang, L. Chen, *Solid State Ionics* **1999**, *121*, 141–156.
[35] E. H. Cha, D. R. Macfarlane, M. Forsyth, C. W. Lee, *Electrochim. Acta* **2004**, *50*, 335–338.
[36] X. Qian, N. Gu, Z. Cheng, X. Yang, E. Wang, S. Dong, *J. Solid State Electrochem.* **2001**, *6*, 8–15.
[37] J. Imbrogno, K. Maruyama, F. Rivers, J. R. Baltzegar, Z. Zhang, P. W. Meyer, V. Ganesan, S. Aoshima, N. A. Lynd, *ACS Macro Lett.* **2021**, *10*, 1002–1007.
[38] B. Natesan, N. K. Karan, R. S. Katiyar, *Phys. Rev. E* **2006**, *74*, 042801.
[39] J. Sun, D. R. Macfarlane, M. Forsyth, *Electrochim. Acta* **1995**, *40*, 2301–2304.
[40] J. Sun, M. Forsyth, D. R. MacFarlane, *J. Phys. Chem. B* **1998**, *102*, 8858–8864.
[41] L. Li, Y. Shan, F. Wang, X. Chen, Y. Zhao, D. Zhou, H. Wang, W. Cui, *ACS Appl. Mater. Interfaces* **2021**, *13*, 48525–48535.
[42] K. M. Diederichsen, E. J. McShane, B. D. McCloskey, *ACS Energy Lett.* **2017**, *2*, 2563–2575.
[43] K. M. Abraham, Z. Jiang, B. Carroll, *Chem. Mater.* **1997**, *9*, 1978–1988.
[44] Y. Lu, M. Tikekar, R. Mohanty, K. Hendrickson, L. Ma, L. A. Archer, *Adv. Energy Mater.* **2015**, *5*, 1402073.
[45] G. Bucci, T. Swamy, Y.-M. Chiang, W. C. Carter, *J. Mater. Chem. A* **2017**, *5*, 19422–19430.
[46] I. Nicotera, L. Coppola, C. Oliviero, G. A. Ranieri, *Ionics* **2005**, *11*, 87–94.
[47] A. Reiche, J. Tübke, R. Sandner, A. Werther, B. Sandner, G. Fleischer, *Electrochim. Acta* **1998**, *43*, 1429–1434.
[48] X. Zou, Q. Lu, Y. Zhong, K. Liao, W. Zhou, Z. Shao, *Small* **2018**, *14*, 1801798.
[49] T. Chen, J. Zhou, G. Fang, Y. Tang, X. Tan, A. Pan, S. Liang, *ACS Sustainable Chem. Eng.* **2018**, *6*, 7250–7256.
[50] A. M. Nolan, Y. Liu, Y. Mo, *ACS Energy Lett.* **2019**, *4*, 2444–2451.
[51] K. N. Wood, E. Kazyak, A. F. Chadwick, K.-H. Chen, J.-G. Zhang, K. Thornton, N. P. Dasgupta, *ACS Cent. Sci.* **2016**, *2*, 790–801.
[52] F. Ye, X. Zhang, K. Liao, Q. Lu, X. Zou, R. Ran, W. Zhou, Y. Zhong, Z. Shao, *J. Mater. Chem. A* **2020**, *8*, 9733–9742.
[53] G. Bieker, M. Winter, P. Bieker, *Phys. Chem. Chem. Phys.* **2015**, *17*, 8670–8679.
[54] G. M. A. Girard, X. Wang, R. Yunis, D. R. MacFarlane, A. J. Bhattacharyya, M. Forsyth, P. C. Howlett, *Batteries & Supercaps* **2019**, *2*, 229–239.
[55] L. Guo, F. Huang, M. Cai, J. Zhang, G. Ma, S. Xu, *ACS Appl. Mater. Interfaces* **2021**, *13*, 32886–32893.
[56] F. Shi, A. Pei, T. Boyle David, J. Xie, X. Yu, X. Zhang, Y. Cui, *Proc. Nat. Acad. Sci.* **2018**, *115*, 8529–8534.
[57] H. Kahlert, U. Retter, H. Lohse, K. Siegler, F. Scholz, *J. Phys. Chem. B* **1998**, *102*, 8757–8765.
[58] P. G. Kitz, M. J. Lacey, P. Novák, E. J. Berg, *J. Anal. Chem.* **2019**, *91*, 2296–2303.
[59] C. Masquelier, A. K. Padhi, K. S. Nanjundaswamy, J. B. Goodenough, *J. Solid State Chem.* **1998**, *135*, 228–234.
[60] A. K. Padhi, K. S. Nanjundaswamy, J. B. Goodenough, *J. Electrochem. Soc.* **1997**, *144*, 1188–1194.
[61] B. Bulut Kopuklu, A. Gomez-Martin, M. Winter, T. Placke, R. Schmuch, S. Alkan Gursel, A. Yurum, *ACS Sustainable Chem. Eng.* **2021**, *9*, 12560–12574.
[62] K. Karki, Y. Huang, S. Hwang, A. D. Gamalski, M. S. Whittingham, G. Zhou, E. A. Stach, *ACS Appl. Mater. Interfaces* **2016**, *8*, 27762–27771.
[63] L. Wu, K.-W. Nam, X. Wang, Y. Zhou, J.-C. Zheng, X.-Q. Yang, Y. Zhu, *Chem. Mater.* **2011**, *23*, 3953–3960.

Manuscript received: June 3, 2022
Revised manuscript received: August 21, 2022
Accepted manuscript online: August 31, 2022
Version of record online: September 12, 2022